Kinetic Modeling of Nernst Effect in Magnetized Hohlraums

A.S. Joglekar*
Particle-In-Cell and Kinetic Simulation Center, University of California - Los Angeles

C. P. Ridgers
York Plasma Institute, University of York, UK

R. J. Kingham
Blackett Laboratory, Imperial College, London, UK

A.G.R. Thomas†
Department of Nuclear Engineering and Radiological Sciences, University of Michigan, Ann Arbor, MI, USA
(Dated: April 4, 2016)

We present nanosecond timescale Vlasov-Fokker-Planck-Maxwell modeling of magnetized plasma transport and dynamics in a hohlraum with an applied external magnetic field, under conditions similar to recent experiments. Self-consistent modeling of the kinetic electron momentum equation allows for a complete treatment of the heat flow equation and Ohm's Law, including Nernst advection of magnetic fields. In addition to showing the prevalence of non-local behavior, we demonstrate that effects such as anomalous heat flow are induced by inverse bremsstrahlung heating. We show magnetic field amplification up to a factor of 3 from Nernst compression into the hohlraum wall. The magnetic field is also expelled towards the hohlraum axis due to Nernst advection faster than frozen-in-flux would suggest. Non-locality contributes to the heat flow towards the hohlraum axis and results in an augmented Nernst advection mechanism that is included self-consistently through kinetic modeling.

There has been recent interest in the role of applied magnetic fields in high-energy-density plasmas [1–3] for inertial fusion energy applications [4]. The Magneto-Inertial Fusion Electric Discharge System has been developed to provide steady state magnetic fields for long time-scales relative to the experiments. An experiment on the Omega Laser Facility with a 7.5 T external axial magnetic field imposed on an Omega-scale hohlraum measured a rise in observed temperature along the hohlraum axis [5] and modeling showed that external fields can guide hot electrons from laser-plasma interactions [6] through the hohlraum, rather than the capsule [7].

From Ohm's Law, it has been shown that electron heat transport advects such magnetic fields through the Nernst effect [8–14] in addition to well-known processes like "frozen-in-flow" and resistive diffusion. Dimensionless numbers comparing the ratio of the magnitudes of the Nernst term to the bulk plasma flow term, $R_N \gg 1$ [10], and the Hall term, $H_N \gg 1$ [13], suggest that Nernst convection should be the dominant mechanism for magnetic field transport in a hohlraum. Such a hot and semi-collisional environment is, however, rich in non-equilibrium effects that may complicate the magnetic field dynamics.

Laser heating of the plasma results in steep temperature gradients, typically $\mathcal{O}(3\,\mathrm{keV}/50\,\mu\mathrm{m})$. The collisional mean-free-path of a 3 keV electron is $\mathcal{O}(10\,\mu\mathrm{m})$, depending on the plasma density. Since $\lambda_{\mathrm{mfp}}/L < 100$, non-locality can be expected to be important [15]. The steep temperature gradients caused by intense laser heating in a hohlraum have been shown to result in non-local heat flow [16, 17]. Careful consideration of the electron population with $2v_{\mathrm{th}} < v < 4v_{\mathrm{th}}$ is required as these carry most of the heat. Additionally, inverse-bremsstrahlung heating of a plasma [18, 19] not only leads to deviations from Braginskii transport [20], but also new transport terms [21, 22]. Both non-locality and laser heating result in modifications to the distribution function and non-equilibrium behavior that result in breakdown of the classical transport approximations. In order to avoid those approximations, a *kinetic approach* is necessary. This allows for modeling of magnetic field dynamics through a self-consistent and generalized Ohm's Law derived without distribution function approximations.

Using a Vlasov-Fokker-Planck-Maxwell formulation, we show simulations of magnetized, 2D hohlraum-scale plasma including ray-tracing of an Omega-like laser configuration over a nanosecond time-scale. Therefore, this simulation includes self-consistent treatment of the fully kinetic Ohm's Law and non-local effects in heat-flow. The hohlraum is considered without a fuel capsule but a gas fill throughout. Note that radiation transport and "laser-plasma interactions" are neglected in these calculations. While these may modify the magnitude of the electron temperature near the high density plasma, the conclusions presented here primarily arise as a result of the non-local dynamics prevalent within the low density, optically thin, gas fill where the radiation effects will

* archis@ucla.edu
† agrt@umich.edu

be negligible [23]. With the use of IMPACTA [24, 25], we studied the effect of non-equilibrium electron kinetics on thermal energetic and magnetic field dynamics of a Omega-scale hohlraum with an externally imposed 7.5 T magnetic field. We found that significant proportions of the total heat flow are non-local. Additionally, presence of inverse bremsstrahlung heating resulted in anomalous heat flow towards the over-dense plasma of the hohlraum wall. Therefore, the diffusive heat flow from the laser-heated regions is not an adequate description of the thermal energetics. Heat flow from the laser heating moves the externally imposed magnetic field through Nernst advection. To examine the effects of Nernst advection in relation to plasma bulk flow, we show modeling without an electron contribution to the transport of magnetic field in Ohm's Law for comparison.

We find that magnetic field transport due to Nernst flow results in significantly faster field cavitation than via frozen-in-flux. The field cavitation occurs due to non-local heat flow towards the hohlraum axis. Retention of the distribution function allows for accurate modeling of the magnetic field pile-up because the local approximation of the Nernst velocity underestimates the true velocity by a factor of 2. Nernst flow into the over-dense region causes flux pile-up at the walls and results in magnetic field amplification by a factor of 3.

The Vlasov-Fokker-Planck equation for electrons given by

$$\left[\frac{\partial}{\partial t}+\mathbf{v}\cdot\frac{\partial}{\partial \mathbf{x}}+\frac{e}{m_e}\left(\mathbf{E}+\mathbf{v}\times\mathbf{B}\right)\cdot\frac{\partial}{\partial \mathbf{v}}\right]f(\mathbf{v},\mathbf{r},t)= -\frac{\partial}{\partial \mathbf{v}}\cdot\{f(\mathbf{v},\mathbf{r},t)\langle\Delta\mathbf{v}\rangle\}+\frac{1}{2}\frac{\partial}{\partial \mathbf{v}}\frac{\partial}{\partial \mathbf{v}}:\{f(\mathbf{v},\mathbf{r},t)\langle\Delta\mathbf{v}\Delta\mathbf{v}\rangle\}, \quad (1)$$

is coupled with Ampere's and Faraday's Laws and a hydrodynamic ion fluid model to describe the plasma. The code we use, IMPACTA [24, 25], uses a Cartesian tensor expansion, with the distribution function expanded as $f(t,\mathbf{r},\mathbf{v}) = f_0 + \mathbf{f}_1\cdot\hat{\mathbf{v}} + \underline{\underline{\mathbf{f}}}_2 : \hat{\mathbf{v}}\hat{\mathbf{v}} + \ldots$, where $\hat{\mathbf{v}}(\theta,\phi)$ is a unit velocity vector. This expansion can be truncated in collisional plasma, as collisions smooth out angular variations resulting in a nearly isotropic distribution, represented by f_0. Higher orders are successively smaller perturbations, $f_0 \gg \mathbf{f}_1 \gg \underline{\underline{\mathbf{f}}}_2$ etc. In the classical limit that f_0 is a Maxwell-Boltzmann velocity distribution, IMPACTA has been shown to agree with Braginskii's transport equations [24]. These simulations, however, are collisional enough such that $\underline{\underline{\mathbf{f}}}_2$ is neglected to an error $\mathcal{O}(\lambda_{\rm mfp}/L)^2$.

A 2-dimensional slice of a hohlraum is modeled in the x-y plane where the y-axis represents the longitudinal axis of the hohlraum and the fuel pellet would sit at the origin. The hohlraum walls are represented by dense, high-Z plasma located at approximately $x = \pm 800$ μm, and the gas fill by low-Z plasma, with the overall Z distribution described by $Z(x,y) = 59.25 + 19.75\tanh(\frac{x-750}{40})$. Electron number density is described by $n_e(x,y) = (2.98 + 2.93\tanh(\frac{x-750}{40})) \times 10^{22}$ cm^{-3}. The initial uniform temperature was $k_B T_{e0} = 160$ eV. The initial uniform magnetic field was $\mathbf{B}_0(\hat{y}) = 7.5$ T and $\ln\Lambda_{ei} = 5.4$. To convert from the normalized units, $n_{e0} = 5\times10^{20}$ cm^{-3} and $v_{\rm th0}/c = 0.025$ are used. The laser parameters resemble those of ref. [5]. The ray tracing package tracks the three beam cones that enter at 21, 42, and 59 deg from the axis, to their respective refraction points.

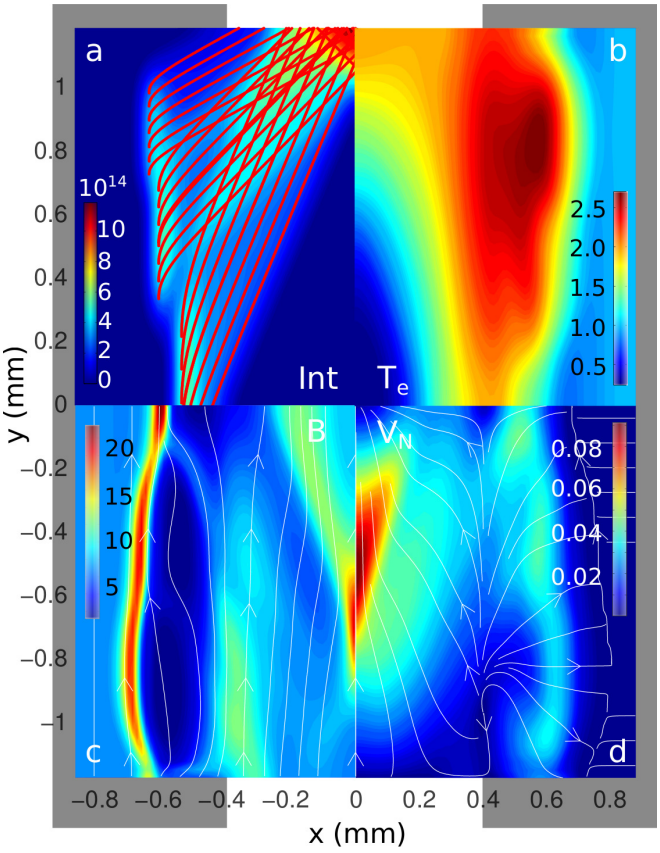

FIG. 1: (a) Ray tracing profile overlaid onto laser intensity profile (W/cm^2) at t = 0. (b) Electron Plasma Temperature (keV), (c) Externally applied magnetic field (T), (d) Nernst Velocity ($v_N/v_{\rm th0}$) at t = 250 ps.

The rays and initial heating profile are shown in fig. 1a. Figure 1b shows the temperature profile after 300 ps of laser heating. Figure 1c shows the cavitation and amplification in the in-plane magnetic field profile caused by intense laser heating. The Nernst velocity, shown in fig. 1d, is directed towards the hohlraum axis in the low density gas fill and into the hohlraum wall in the Au plasma. In the rest of this paper, we show that Nernst flow is primarily responsible for the magnetic field profile seen in fig. 1c.

Inverse bremsstrahlung heating of plasma results in a super-Gaussian electron distribution [18], which modifies the transport coefficients [21, 26, 27] and introduces new terms including an anomalous heat flux up a pressure

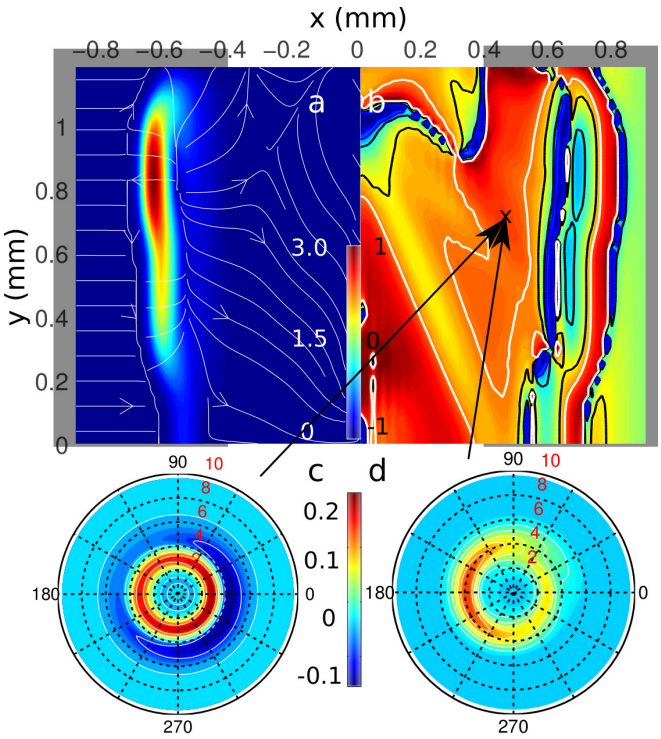

FIG. 2: (a) Heat flow $(m_e n_{e0} v_{\rm th0}^3)$ (b) $1 - q_{\rm eq.\ (2)}/q_{\rm code}$ (c) $v^5(f_{\rm code} - f_{\rm MB})$ (d) $v^5(f_{\rm code} - f_{\rm SG})$ @ $x = 0.4$ mm, $y = -0.6$ mm, $m = 2.625$, $t = 100$ ps.

gradient $\mathbf{q}_n$, represented by the last term in

$$\mathbf{q}_e = -\frac{T_e}{e}\underline{\underline{\psi'}} \cdot \mathbf{j} - \left(\underline{\underline{\kappa}} + n_e\underline{\underline{\phi}}\right) \cdot \nabla T_e - T_e\underline{\underline{\phi}} \cdot \nabla n_e \ , \quad (2)$$

where ψ, ϕ and κ are transport coefficients. These are functions of the local magnetic field, current, and temperature gradients and density gradients, as described in ref. [21]. Equation (2) recovers the calculation from ref. [26] in the limit where f_0 is a Maxwell-Boltzmann velocity distribution. $\mathbf{q}_n$ increases as $m > 2$ increases, where m is the power of the super-Gaussian distribution function defined by $f_{\rm SG}(v) = C(m) n_e / v_{\rm th}^3 \exp\left(-(v/\alpha_e v_{\rm th})^m\right)$ where $\alpha_e = [3\Gamma(3/m)/2\Gamma(5/m)]^{1/2}$ and $C(m) = m/4\pi\alpha_e^3\Gamma(3/m)$.

In these simulations, by finding the best fit of a super-Gaussian distribution to the low-velocity part of f_0, m reaches a maximum of 3.1 near the centers of the laser heated regions, but varies spatially and temporally, thus requiring the preservation of the distribution function at each point throughout the simulation for accurate calculation of the heat flow. Using theory detailed in refs. [21, 27], the heat flow can be modified in hydrodynamics codes to include this effect. However, the distribution is not precisely a super-Gaussian [28] due to other effects such as non-locality, magnetic-fields, and collisions and this fix remains an approximation.

A post-processed calculation of the anomalous heat flow shows that there is heat flow towards the hohlraum wall due to the $\phi\nabla P_e$ term and this approximately results in a 10% correction to the diffusive heat flow i.e. $\kappa\nabla T_e$.

A majority of disagreement between the heat flow from the code and the post-processed heat flow from all three terms from eq. (2) stems from the strongly non-local heat flow that is prevalent in the hohlraum. Figure 2b shows a 2D profile of a metric for quantifying the discrepancy between the two heat flows, described by the relative difference between the super-Gaussian-approximation and the exact heat fluxes, $1 - q_{\rm eq.\ (2)}/q_{\rm code}$.

The regions within black contours have $\pm 25\%$ agreement between the two heat flows. The white contours correspond to regions of high non-locality where the super-Gaussian transport calculation is an underapproximation, while the blue contours correspond to regions where the heat flow is significantly overcalculated. Heat flow from regions near the temperature hotspots, ± 50 μm, is overestimated by the super-Gaussian calculation while the heat flow further away from the hotspots, ± 200 μm, is underestimated, as expected from the existence of non-locality. The regions of relative agreement are $\pm$ 50 − 200 μm from the hot spots.

Consideration of the in-plane electron distribution function $f(\theta, v) = f_0 + f_{1x}\hat{v}_x + f_{1y}\hat{v}_y$ can show the significance of inverse-bremsstrahlung heating and non-locality. Since $\mathbf{q} \propto \int v^5 f(\theta, v)\, \hat{\mathbf{v}}(\theta, \phi)\, dv \sin\theta d\theta d\phi$, the important contributions to the heat flow may be best illustrated by the function $v^5 f(\theta, v)$. Figure 2c and d show the difference between the calculated distribution $v^5 f$ and (c) a Maxwell-Boltzmann $v^5 f_{\rm MB}$ and (d) a super-Gaussian with best fit to m, both with $T_e((x = 0.4, y = -0.6)$. Figure 2c shows that $f > f_{\rm MB}$ in the region $2 < v_{\rm th} < 4$ and $f < f_{\rm MB}$ in the region $4 < v_{\rm th} < 6$, which is characteristic of inverse-bremsstrahlung heating. Calculating the heat flow contribution difference between the real distribution and the best-fit super-Gaussian ($m \approx 2.625$ in this case), shows that the inverse-bremsstrahlung model does not replicate the distribution function fully due to anisotropy from the flow and non-locality. The enhanced tail and shifted center in the 180° direction is characteristic of the (non-local) heat flow down the density gradient while the colder return flow is a result of the features in the 0° direction.

As shown in ref. [9], the Nernst velocity is given by

$$\mathbf{v}_N = \frac{\langle \mathbf{v} v^3 \rangle}{2\langle v^3 \rangle} + \frac{\mathbf{j}}{e n_e}, \quad (3)$$

$$\approx \frac{\underline{\underline{\kappa}} \cdot \nabla T_e}{5/2 P_e}. \quad (4)$$

It can be shown for this geometry that B_y has no field generation terms from the curl of Ohm's Law and therefore, can be transported through $(\mathbf{v}_N + \mathbf{C}) \times \mathbf{B}$ term in addition to resistive diffusion. Over 0.5 ns, the simulation shows that there is magnetic field cavitation resulting in flux pile-up on the hohlraum axis and compression at the hohlraum wall due to the energy deposition from the

laser. Pile-up of magnetic flux results in a 25 T magnetic field, more than 3 times the strength of the initial 7.5 T field.

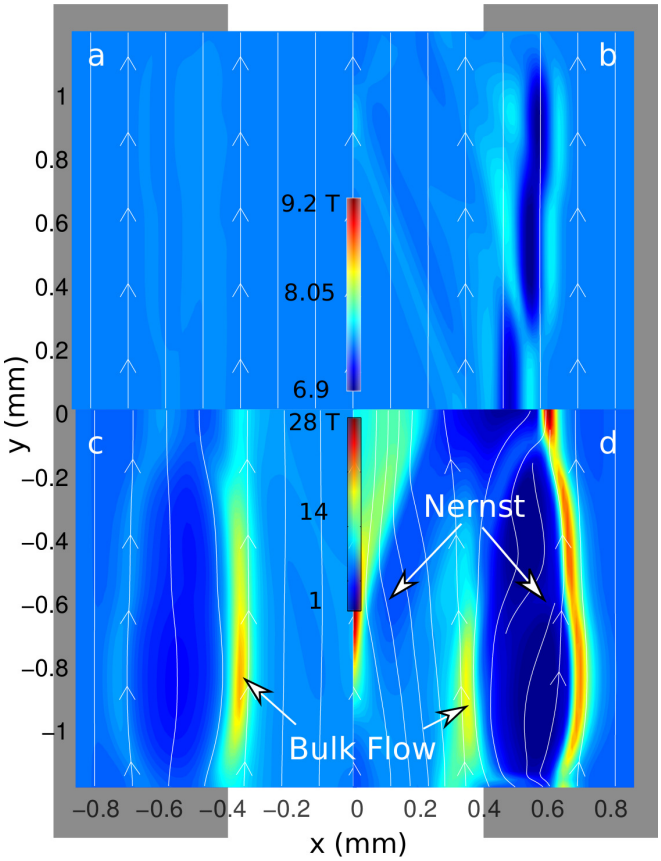

FIG. 3: **B** (T) after 50 ps with only plasma bulk flow (a) and full Ohm's Law (b).
B after 400 ps with only plasma bulk flow (c) and full Ohm's Law (d)

In order to determine the effect of Nernst advection on the magnetic field evolution, simulations with and without the $\mathbf{B} \times \mathbf{f}_1$ term in the $\mathbf{f}_1$ equation were compared. This term is responsible for the interaction of kinetic electrons with the magnetic field, therefore, responsible for the Nernst and Hall terms in Ohm's Law as well as the Righi-Leduc effect in the heat flow equation. Simulations agree with the previous determination that $\mathbf{j} \ll \mathbf{v}_N$ because $H_N \ll 1$ and the Hall effect can be neglected. The magnetic field after 50 ps without and with full Ohm's Law treatment is shown in fig. 3a and fig. 3b, respectively. The field has been expelled from the laser heated region in both cases but the magnitudes differ. It is not evident in fig. 3a since the field is only modified by a few percent by the plasma bulk flow. Thermal energy transport results in a more noticeable change immediately over 50 ps.

An estimate of the time-scale for plasma bulk flow to transport frozen-in magnetic fields to the hohlraum axis is given by, $\frac{r_H}{C_s} \approx \frac{r_H}{\sqrt{k_B T_e / M_i}} \sim 2$ ns. Figure 3d shows that including the Nernst effect results in magnetic field cavitation on a faster time-scale than can be expected due to field advection only through bulk plasma flow in fig. 3c. Given a 7.5 T initial field strength, the magnetic field on the axis grows to 30 T within 0.5 ns. Figure 3d also shows that the magnetic flux pile-up in the hohlraum wall occurs due to the Nernst effect, increasing to a strength of nearly 25 T towards the hohlraum wall.

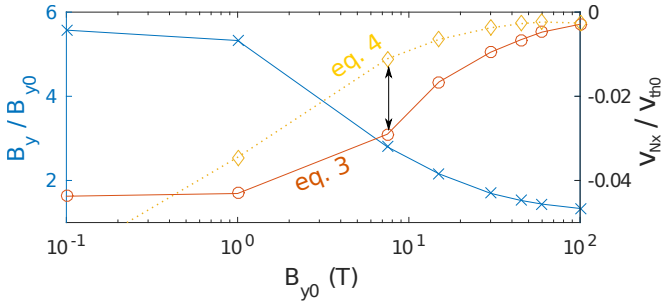

FIG. 4: Magnetic field at the hohlraum axis decreases as applied field strength is increased because the Nernst effect is mitigated, preventing the magnetic field from accumulating near the hohlraum axis. (t = 300 ps). The discrepancy between the approximated and exact Nernst velocity also decreases.

We ran a series of simulations with varying initial applied field B_{y0} to understand how field strength affects the hohlraum dynamics. Figure 4 shows results of these simulations suggesting the limiting behavior as the magnetic field is increased is given by

$$\lim_{B_{y0} \to \infty} B_{y-\text{axis}} / B_{y0} = 1. \tag{5}$$

The maximum value of v_N in the domain of magnetic field advection towards the axis (-0.5 mm $< x <$ 0.5 mm) is chosen. This trend can be explained by the observed reduction in the Nernst velocity towards the hohlraum axis as the magnetization increases (also shown in fig. 4), which quenches magnetic field transport. These $v_N(\omega\tau)$ curves are in line with other predictions [9, 13, 21] that $v_N \propto 1/\omega\tau$ for $\omega\tau \gg 1$. Figure 4 also shows that the exact Nernst velocity from eq. (3) is consistently, and up to 2×, larger than what the local approximation from eq. (4) would predict for T_e, n_e, and **B** profiles at 300 ps. This discrepancy decreases at higher field strengths due to magnetic field induced localization of the heat flow carrying electrons.

The degree of magnetic flux pile up in the hohlraum wall, however, is not affected strongly by the increase in magnetic field strength because $\omega\tau \sim n_e^{-1}$. The magnitude of maximum field strength in the wall ranges from $2 < B_y/B_{y0} < 3$ for $1 < B_{y0} < 100$ T.

IMPACTA is in agreement with the HYDRA modeling performed in [5] with respect to the hydrodynamic motion of the plasma only. In that sense, the hydrodynamic ion model that is coupled to the electron transport model in IMPACTA agrees. While it is not possible to compare

the modeling in the two works directly, the IMPACTA modeling seeks to highlight the fact that magnetic field transport in [5] is inadequate because it does not include Nernst convection.

We have shown Vlasov-Fokker-Planck modeling of external magnetic fields of 1-100 T imposed upon an Omega-scale hohlraum. Magnetic flux pile-up increases the magnetic field magnitude by a factor of 3 for a 7.5 T magnetic field. Additionally, the heat flow is responsible for magnetic field cavitation on a faster time-scale than that from the bulk flow of the plasma. Not only is the heat flow strongly non-local, it also has distinct signatures of inverse bremsstrahlung heating. The ability to preserve distribution function information through use of a kinetic code allows to model the heat flow accurately. Full Vlasov-Fokker-Planck-Maxwell treatment of the system enables accurate modeling of magnetic field dynamics. We have shown that Nernst flow is the dominant mechanism for magnetic field transport and is responsible for the increase in field strength, up to 100 T for a initial 100 T field, in the wall as well as cavitation of the magnetic field towards the hohlraum axis. The field cavitation is mitigated at higher field strengths. Furthermore, the Nernst velocity is up to 2× larger in self-consistent non-local calculations than would be predicted by diffusive transport.

These findings suggest that attempting the same calculation with diffusive transport would result in significantly different $\mathbf{B}$ & T_e evolution. Accurate modeling of these quantities has implications for laser plasma interactions [5, 6] and hot electron propagation [7] in the gas fill and understanding hot spots on the dense plasma that generate X-rays. The kinetic electron transport and $\mathbf{B}$ field physics presented here could affect details of X-ray drive if incorporated into full-scale radiation-hydrodynamics modeling (including reduced phenomenological laser-plasma interaction models) of indirect drive with externally applied B-field.

ACKNOWLEDGMENTS

The authors would like to thank A. Hazi, J. Moody, D. Strozzi of LLNL and A. Sefkow of Sandia for useful discussions regarding related work at NIF and Omega. The modeling was performed using computational resources and services provided by Advanced Research Computing at the University of Michigan, Ann Arbor. This research was supported by the DOE through Grant No. DE SC0010621.

[1] P. Y. Chang, G. Fiksel, M. Hohenberger, J. P. Knauer, R. Betti, F. J. Marshall, D. D. Meyerhofer, F. H. Séguin, and R. D. Petrasso, Physical Review Letters **107**, 035006 (2011).

[2] M. Hohenberger, P. Y. Chang, G. Fiksel, J. P. Knauer, R. Betti, F. J. Marshall, D. D. Meyerhofer, F. H. Séguin, and R. D. Petrasso, Physics of Plasmas **19**, 056306 (2012).

[3] G. Fiksel, W. Fox, A. Bhattacharjee, D. H. Barnak, P. Y. Chang, K. Germaschewski, S. X. Hu, and P. M. Nilson, Physical Review Letters **113**, 1 (2014).

[4] J. D. Lindl, P. Amendt, R. L. Berger, S. G. Glendinning, S. H. Glenzer, S. W. Haan, R. L. Kauffman, O. L. Landen, and L. J. Suter, Physics of Plasmas **11**, 339 (2004).

[5] D. S. Montgomery, B. J. Albright, D. H. Barnak, P. Y. Chang, J. R. Davies, G. Fiksel, D. H. Froula, J. L. Kline, M. J. Macdonald, A. B. Sefkow, L. Yin, and R. Betti, Physics of Plasmas **22**, 010703 (2015).

[6] S. P. Regan, N. B. Meezan, L. J. Suter, D. J. Strozzi, W. L. Kruer, D. Meeker, S. H. Glenzer, W. Seka, C. Stoeckl, V. Y. Glebov, T. C. Sangster, D. D. Meyerhofer, R. L. McCrory, E. A. Williams, O. S. Jones, D. A. Callahan, M. D. Rosen, O. L. Landen, C. Sorce, and B. J. MacGowan, Physics of Plasmas **17**, 020703 (2010).

[7] D. J. Strozzi, L. J. Perkins, M. M. Marinak, D. J. Larson, J. M. Koning, and B. G. Logan, Journal of Plasma Physics **81**, 475810603 (2015), arXiv:1508.00803.

[8] A. Nishiguchi, T. Yabe, M. G. Haines, M. Psimopoulos, and H. Takewaki, Physical Review Letters **53**, 262 (1984).

[9] M. G. Haines, Plasma Physics and Controlled Fusion **28**, 1705 (2000).

[10] C. P. Ridgers, R. J. Kingham, and A. G. R. Thomas, Physical Review Letters **100**, 075003 (2008).

[11] L. Willingale, A. G. R. Thomas, P. M. Nilson, M. C. Kaluza, S. Bandyopadhyay, A. E. Dangor, R. G. Evans, P. Fernandes, M. G. Haines, C. Kamperidis, R. J. Kingham, S. Minardi, M. Notley, C. P. Ridgers, W. Rozmus, M. Sherlock, M. Tatarakis, M. S. Wei, Z. Najmudin, and K. Krushelnick, Physical Review Letters **105**, 1 (2010).

[12] C. K. Li, F. Séguin, J. Frenje, N. Sinenian, M. Rosenberg, M.-E. Manuel, H. Rinderknecht, A. Zylstra, R. Petrasso, P. Amendt, O. Landen, A. Mackinnon, R. Town, S. Wilks, R. Betti, D. Meyerhofer, J. Soures, J. Hund, J. Kilkenny, and A. Nikroo, Nuclear Fusion **53**, 073022 (2013).

[13] A. S. Joglekar, A. G. R. Thomas, W. Fox, and A. Bhattacharjee, Physical Review Letters **112**, 105004 (2014).

[14] L. Lancia, B. Albertazzi, C. Boniface, A. Grisollet, R. Riquier, F. Chaland, K.-C. Le Thanh, P. Mellor, P. Antici, S. Buffechoux, S. N. Chen, D. Doria, M. Nakatsutsumi, C. Peth, M. Swantusch, M. Stardubtsev, L. Palumbo, M. Borghesi, O. Willi, H. Pépin, and J. Fuchs, Physical Review Letters **113**, 235001 (2014).

[15] D. R. Gray, J. D. Kilkenny, M. S. White, P. Blyth, and D. Hull, Physical Review Letters **39**, 1270 (1977).

[16] G. Gregori, S. H. Glenzer, J. Knight, C. Niemann, D. Price, D. H. Froula, M. J. Edwards, R. P. J. Town, A. Brantov, W. Rozmus, and V. Y. Bychenkov, Physical Review Letters **92**, 205006 (2004).

[17] J. Hawreliak, D. M. Chambers, S. H. Glenzer, A. Gouveia, R. J. Kingham, R. S. Marjoribanks, P. a. Pinto, O. Renner, P. Soundhauss, S. Topping, E. Wolfrum, P. E. Young, and J. S. Wark, Journal of Physics B: Atomic,

Molecular and Optical Physics **37**, 1541 (2004).
[18] A. B. Langdon, Physical Review Letters **44**, 575 (1980).
[19] J. M. Liu, J. S. De Groot, J. P. Matte, T. W. Johnston, and R. P. Drake, Physical Review Letters **72**, 2717 (1994).
[20] S. I. Braginskii, Reviews of Plasma Physics **1**, 205 (1965).
[21] C. P. Ridgers, A. G. R. Thomas, R. J. Kingham, and A. P. L. Robinson, Physics of Plasmas **15**, 092311 (2008).
[22] W. Y. Huo and Q. Zeng, Physics of Plasmas **22**, 094503 (2015).
[23] J. Morton, Private Communication (2015).
[24] R. J. Kingham and A. R. Bell, Journal of Computational Physics **194**, 1 (2004).
[25] A. G. R. Thomas, R. J. Kingham, and C. P. Ridgers, New Journal of Physics **11**, 033001 (2009).
[26] E. M. Epperlein and M. G. Haines, Physics of Fluids **29**, 1029 (1986).
[27] J. J. Bissell, C. P. Ridgers, and R. J. Kingham, New Journal of Physics **15**, 025017 (2013).
[28] E. Fourkal, V. Y. Bychenkov, W. Rozmus, R. Sydora, C. Kirkby, C. E. Capjack, S. H. Glenzer, and H. A. Baldis, Physics of Plasmas **8**, 550 (2001).